16th World Conference on Earthquake, 16WCEE 2017
Santiago Chile, January 9th to 13th 2017
Paper N° 792 (Abstract ID)
Registration Code: S-0000013422

Experimental study on the collapse process of an 18-story high-rise steel building based on the large-scale shaking table test

J. Kubota[1], Y. Suzuki[2], K. Suita[3], Y. Sawamoto[4], T. Kiyokawa[5], N. Koshika[6] and M. Takahashi[7]

[1] *Chief Research Engineer, Building Structures Group, Kajima Technical Research Institute, jkubota@kajima.com*
[2] *General Manager, Structural Research Department, Kobori Research Complex Inc., y-suzuki@kobori-takken.co.jp*
[3] *Professor Dr. Eng., Department of Architecture and Architectural Engineering, Kyoto University, suita@archi.kyoto-u.ac.jp*
[4] *Chief Research Engineer, Building Structures Group, Kajima Technical Research Institute, sawamoto@kajima.com*
[5] *Research Engineer, Building Structures Group, Kajima Technical Research Institute, kiyokawt@kajima.com*
[6] *Deputy Manager, Kobori Research Complex Inc., Koshika@kobori-takken.co.jp*
[7] *General Manager Dr. Eng., Building Structures Group, Kajima Technical Research Institute, motomi@kajima.com*

Abstract

This paper reports on a large-scale shaking table test of a high-rise steel building conducted at the facility called E-Defense. The building specimen is a 1/3-scale 18-story steel moment frame. The input motions were based on the expected long-period and long-duration strong earthquake. The specimen was subjected to a series of progressively increasing scaled motions until it completely collapsed. The damage of the steel frame began through the yielding of beams along lower stories and column-bases of the first story. After several excitations by increasing scaled motions, cracks initiated at the welded moment connections and fractures in the beam flanges spread to the lower stories. As the shear strength of each story decreased, the drifts of lower stories increased and the frame finally collapsed. From the test results, the typical collapse progression for a tall steel moment frame was obtained, and the hysteretic behaviors of steel structural members including deterioration due to local buckling and fracture were observed.

Keywords: High-rise building, Long-period ground motion, Shaking table test, Collapse behavior

1. Introduction

The importance of precaution to unexpected earthquakes was highlighted by the 2011 Great East Japan Earthquake. High-rise buildings in urban areas are playing important roles for everyday life and business. This study's destination is to evaluate the collapse margin for steel structures of such buildings [1].

A number of experimental and analytical studies on collapse behavior have been conducted in the past work [2]. Collapse tests of 4-story steel moment resisting frames having two different scales [3], shaking table test of a full-scale 4-story steel moment resisting frame [4] conducted at the E-Defense at the Hyogo Earthquake Engineering Research Center of Japan's National Research Institute for Earth Science and Disaster Prevention [5], and large-scale shaking table test of a high-rise steel building consisted of a 4-story steel moment resisting frame and three substituted layers placed on the top of the moment frame [6] have been carried out. And many component experiments have been conducted to predict the collapse of buildings [7] and component models have been proposed for the collapse analyses [7-13].

In those previous experimental studies, the specimens had only several floors, also were small and the actual welding conditions could not be considered. The component experiments were carried out independently, and the successively-occurring damages were not examined in the whole building.

In this study, a large-scale shaking table test was carried out to clarify the collapse process for a high-rise steel building (Fig. 1, 2) conducted at the E-Defense. The specimen is a 1/3 scale 18-story steel moment frame designed based on the Japanese design standard in the 1980s and 1990s. The input motion is a hypothetical long-period and long-duration strong ground motion observed during a coinstantaneous earthquake typical of Tokai, Tonankai, and Nankai. In the test, the damage progress of columns, beams and beam-to-column moment connections was observed and the overall building behavior in response to simultaneous damage to multiple components was clarified. Finally, the collapse process of the test specimen was examined.

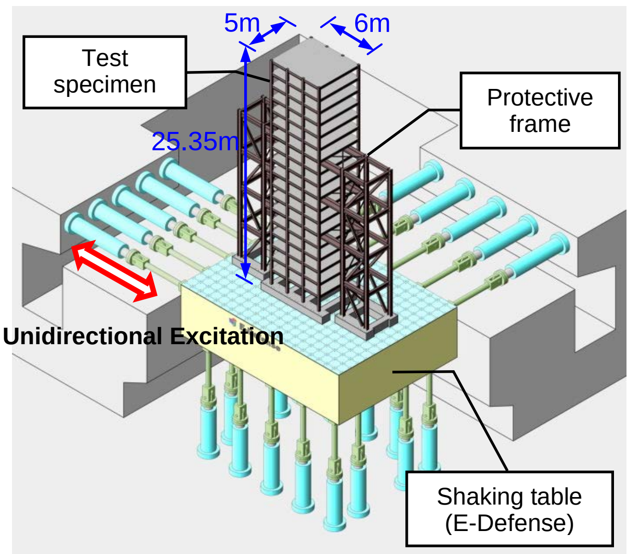

Fig. 1 – Shaking-table test at E-Defense

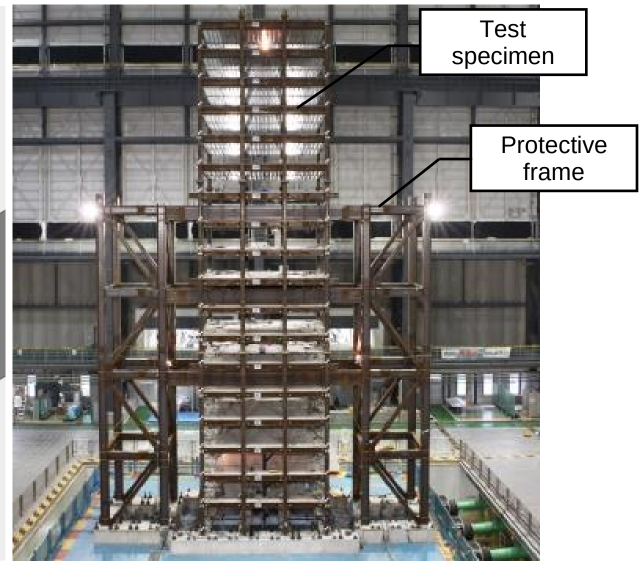

Fig. 2 – Panoramic view of the specimen

2. Specifications of the test specimen

The test specimen was 1/3-scale 18-story steel moment frame whose plan dimensions were 6 m in the input direction and 5 m in the orthogonal direction, and the total height was 25.35 m (Fig. 3). The story heights were 1.70 m (first story), and 1.35 m (2nd–18th stories). The aspect ratio of the frame was approximately 4.2 (= 25.35/6). The total weight of the specimen is 3800 kN (not including foundation).

The test specimen was designed based on the Japanese design standard in the 1980s and 1990s. The base shear coefficient of the frame at the plastic collapse mode defined by plastic hinges at beam ends is 0.45. This value is relatively larger than the design level since the sections of main members are increased to satisfy the requirement of maximum drift to be less than 0.01 rad. The column overdesign ratio was more than 1.5. Built-up square tube columns were used from the 2nd to 7th stories and cold-formed square tube columns were used from 8th to 18th stories. Wide-flange sections of beams were connected to columns by the site-welding method, i.e., the flange-welded and the web-bolted type and the adequate diaphragm plates were inserted in the section of square tube columns at the location of the joint with flanges of beams. The details of welded moment connections (Fig. 4) and welding practices were typical style before the 1995 Hyogoken-Nanbu Earthquake. Columns were made of SM490A steel, where the nominal yield strength was 325 N/mm^2 and tensile strength was 490 N/ mm^2 (stories 1st–6th) and BCR295 steel, where the nominal yield strength was 295 N/mm^2 and tensile strength is 490 N/ mm^2 (stories 7th–18th). The beams were made of SM490A steel similar to the column (welded H-shaped cross section). Table 1 gives the results of steel tensile testing. The fracture toughness of beams obtained from charpy impact test was 200J at 0^{o}C having the high quality to prevent brittle fractures.

The specimen consisted of two parallel three-bay plane frames connected by beams in the orthogonal direction. The shaking table test was conducted in one direction being parallel to the direction of two plane test frames. Therefore, bi-axial behavior of the frame and columns were not examined in this experiment. A reinforced concrete slab, 50 mm depth, was settled on each floor and jointed with beams by stud bolts to obtain the sufficient in-plane stiffness of the floor and the composite action with beams. The total weight of the floor was set as 7 kN/m^2 and, in order to properly simulate the gravity and the inertia forces, the additional concrete plates were suspended under the floor slab. The ratios of axial force to yield strength of columns were 0.12 (outer columns) and 0.16 (inner columns) by long-term load, where this value is relatively smaller than the design level and 0.58 and 0.52 during seismic response at the first story. By using flexural full plastic strength of columns considering axial force, the column overdesign ratio during seismic response was 1.53 to 1.62 being almost the same as the design target value. The protective frame was used to prevent the shaking table from damage during collapse test. This frame had sufficient stiffness to be regarded as rigid.

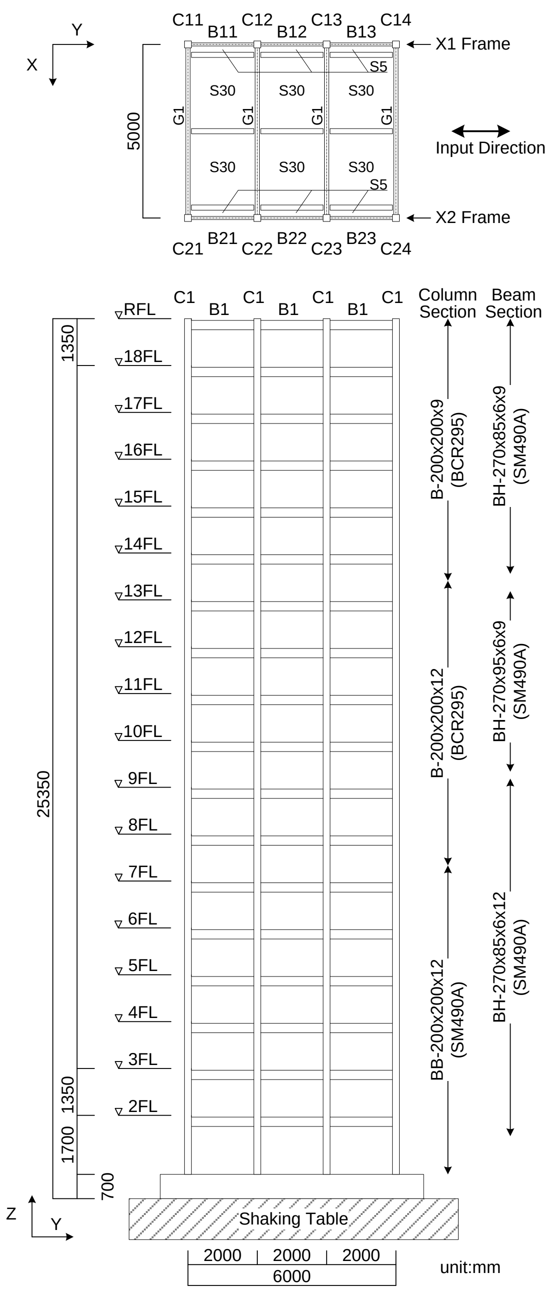

Fig. 3 –Floor plan and elevation of test specimen

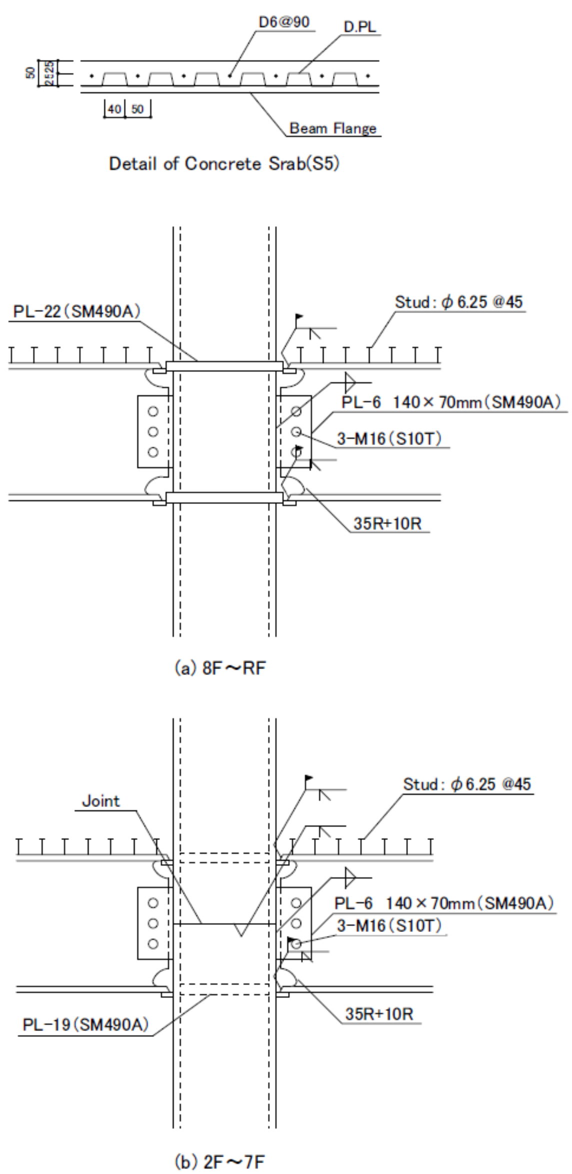

Fig. 4 – Beam-to-column connections

Table 1 Tensile test results

	Material	Part	t mm	Test Piece ※1	Note	Upper yield stress N/mm²	Lower yield stress N/mm²	Tensile strength N/mm²	Elongation %	Yield ratio %	Reduction of area %
Column	SM490A	C1	12	1A	BB-1	384	374	523	27	73	71
					BB-2	382	364	524	28	73	71
					BB-3	384	360	521	28	74	73
	BCR295	C1	12	1A	2C-1	437	420	467	20	94	-
					2C-2	431	425	467	21	92	-
					2C-3	435	423	468	19	93	-
	BCR295	C1	9	1A	3C-1	438	423	457	23	96	-
					3C-2	445	418	458	26	97	-
					3C-3	430	405	455	19	95	-
Beam	SM490A	B1	12	1A	B1-1	393	372	540	28	73	60
					B1-2	397	364	541	25	73	58
					B1-3	392	364	538	26	73	-
	SM490A	B1	9	1A	B1-4	385	368	540	25	71	-
					B1-5	385	368	540	25	71	-
					B1-6	383	365	539	28	71	-
					B1-7	384	364	539	27	71	-
					B1-8	384	368	538	25	71	-
					B1-9	387	369	537	26	72	-
	SM490A	B1	6	1A	B1-10	476	445	572	19	83	56
					B1-11	478	449	575	20	83	56
					B1-12	475	438	568	20	84	56

※1:Japanese industrial standards(JIS Z 2201)

3. Input ground motion

The input motion is a hypothetical long-period and long-duration strong ground motion observed during a coinstantaneous earthquake typical of Tokai, Tonankai, and Nankai[15]. The earthquake is assumed to the most significant impact on the high-rise buildings in urban areas. The spectrum of the long-period ground motion was assumed to be flat in the frequency domain to predict the response accuracy before the test and evaluate them afterward. For the input's phase properties, observation data recorded in Tokyo during the 2011 Great East Japan Earthquake were adopted. Fig. 5 and 6 show the velocity time history, the velocity spectrum and the energy spectrum. In the shaking test, the time scale of the ground motion is shortened to $(1/3)^{0.5}$ based on the similitude laws. In each vibration, the amplitude was multiplied by the factor. The vibration schedule is given in Table 2. The vibration schedule was set in order to collapse the test specimen completely, not assumed an actual earthquake.

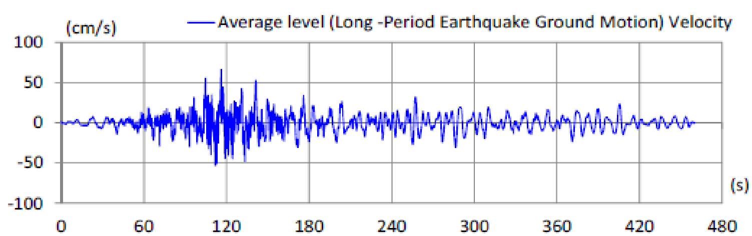

Fig. 5 – Velocity time history of simulated long-period ground motion

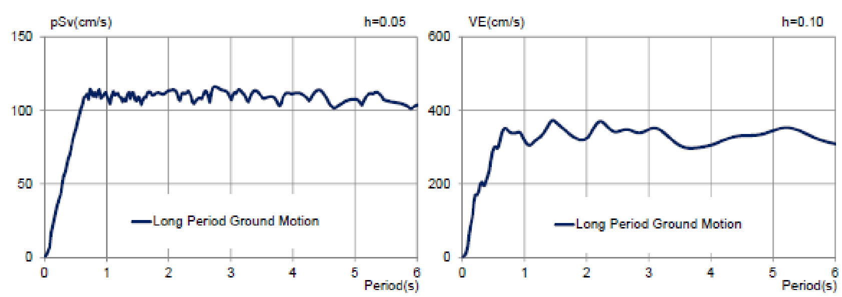

Fig. 6 – Response and energy spectrum of simulated ground motion(average level)

4. Test results

4.1 Overall building behavior

Results of shaking table tests are summarized in the table 2. The specimen collapsed at the lowest four stories is shown in Fig. 7.

The overall building behavior is shown in Fig. 8 for the representative excitations. The results of absolute accelerations (Fig. 8(a)) show appreciable responses for the second modal vibration as well as for the first. As the excitation level rose, the second modal vibration is reduced, and at levels exceeding pSv300, the maximum response from the upper story to the lower story was mostly constant. Even when input acceleration was high, the top-story response was limited and a diminishing tendency was seen. The relative displacement (Fig. 8(b)) increased according to the story height until an excitation level of pSv220 was reached. Then at values exceeding pSv300, displacement in the first–sixth-story range was dominant throughout the building, and displacement remained concentrated in the lower stories. The drift angle (Fig. 8(c)) was calculated using 1) acceleration integral calculus for the 12th story and above, 2) data from wire-type displacement meters on the 12th story and below, and 3) data from laser-type displacement meters on the first to third stories. Story height was considered in the calculation. The distribution of the drift angle was similar for all stories up to an excitation level of pSv220. Deformation was concentrated on lower stories at levels exceeding pSv300 (1/30 at pSv300, 1/16 at pSv340-1 and 1/10 at pSv420-1). In contrast to the lower stories, where deformation was concentrated, no increasing tendency of deformation was observed on the upper stories. Their maximum story drift angles were remained around 1/50. The inertial force for each story was calculated from the acceleration of individual stories, and the inertial forces were added downwards from the top of the building sequentially to calculate the story shear force. The story shear force (Fig. 8(d)) increased with the excitation level in the range from pSv110-1 to pSv180-1. The story shear force coefficient was 0.37 and 0.46 for pSv110-1 and pSv180-1, respectively. Then the shear force approached a limit at pSv220 and reached its maximum at pSv300, after gradual decrease was seen. This tendency is attributed to the degradation of horizontal resistance due to the beam-end fracture and the local buckling in columns, and to the degradation of apparent horizontal resistance due to the PD effect.

The time history of the horizontal displacement on the 12th floor (Fig. 9) was determined using a wire-type displacement meter. As the input excitation amplitude increased through the instances of pSv110-1, pSv180-1 and pSv220, the maximum deformation also increased. However, owing to the plasticity of the model's components, maximum deformation increased less than the expectation from the input excitation level. There was also little residual deformation. At an excitation level of pSv300, the vibration characteristics and timing of maximum deformation differed from those observed at pSv220. The extension of the vibration period was observed in the latter half of vibrations in particular, and there was notably little vibrations after 180 s. Residual deformation was also observed on the negative side. At an excitation level of pSv340-1, extension of

Table 2 Shaking table test results

Excitation Level	% to pSv110	Legends		Top Floor Displacement (cm)	Max.StoryDefl. Angle	Damage
pSv40cm/s	36.4%	pSv40	Design(Elastic)	8.5	1/171 (14F)	elastic
pSv81cm/s	73.6%	pSv81	Design(Plastic)	15.3	1/110 (3,14F)	plastic(2-4FL beams)
pSv110cm/s	100.0%	pSv110-1	Average Level*1	20.6	1/90 (14F)	plastic(2-7FL beams and 1F columns)
pSv110cm/s	100.0%	pSv110-2	Average Level*1	21.7	1/91 (14F)	ditto
pSv180cm/s	163.6%	pSv180-1	Maximum Level*1	30.8	1/62 (11F)	plastic(2-14FL), sign of crack(2-5FL)
pSv180cm/s	163.6%	pSv180-2	Maximum Level*1	31.7	1/55 (11F)	plastic(2-14FL), crack(2-5FL)
pSv220cm/s	200.0%	pSv220	over Maximum Level*1	34.7	1/48 (9F)	fracture(2FL)
pSv250cm/s	227.3%	pSv250	over Maximum Level*1	33.7	1/45 (2F)	fracture(2-3FL)
pSv300cm/s	272.7%	pSv300	over Maximum Level*1	37.4	1/30 (2F)	fracture(2-5FL)
pSv340cm/s	310.0%	pSv340-1	over Maximum Level*1	51.0	1/16 (2F)	progress of fracture to upper floors, local buckling of 1FL column
pSv340cm/s	310.0%	pSv340-2	over Maximum Level*1	56.3	1/13 (2F)	
pSv420cm/s	381.8%	pSv420-1	over Maximum Level*1	66.6	1/10 (2F)	fracture of all beams(2-6FL), local buckling of 1F column
pSv420cm/s	381.8%	pSv420-2	over Maximum Level*1	100	1/6 (2F)	
pSv420cm/s	381.8%	pSv420-3	over Maximum Level*1	Collapse	Collapse	

*1: Long Period Ground Motion at Aichi Pref. when Nankai-Trough Eartuquake the vibration period was observed from the first half of the shaking period, and vibration in the latter half was greater than that observed at pSv300. At pSv420-1, residual deformation turned from negative to positive, and at pSv420-2 it increased appreciably from 25 cm at the onset of vibration to 100 cm at the end. Finally, at pSv420-3, the test specimen suddenly began to vibrate on the positive side about 60 s after the onset of vibration and the deformation range exceeded the horizontal clearance between the test specimen and protective frame. It subsequently leaned against the protective frame, and the specimen was considered to have reached a state of collapse.

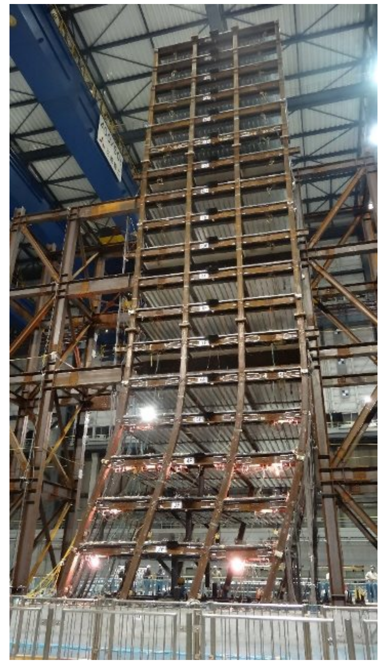

Fig. 7 – Collapse of lower story(pSv420-3)

4.2 Behavior of story

The story shear force-drift angle relationships of the second story are shown in Fig. 10. At an excitation level of pSv110-1, small amount of energy was absorbed by the plasticity of individual elements. At pSv180-1, the shear force and drift angle increased, as did absorption energy. At pSv220, hysteretic damping increased although the maximum shear force did not change appreciably from that observed at pSv180-1. At pSv300, deterioration was observed and the shear force decreased even for the same deformation. Additionally, the hysteresis loop was similar to the shape of a reverse "S". Appreciable deterioration was observed at pSv340-1, and hysteresis had a tendency toward the maximum point experienced in the past. At pSv420-1, the shear force deteriorated additionally and the recovery of the stiffness in large drift angle became negligible. The maximum shear force was around 1400 kN.

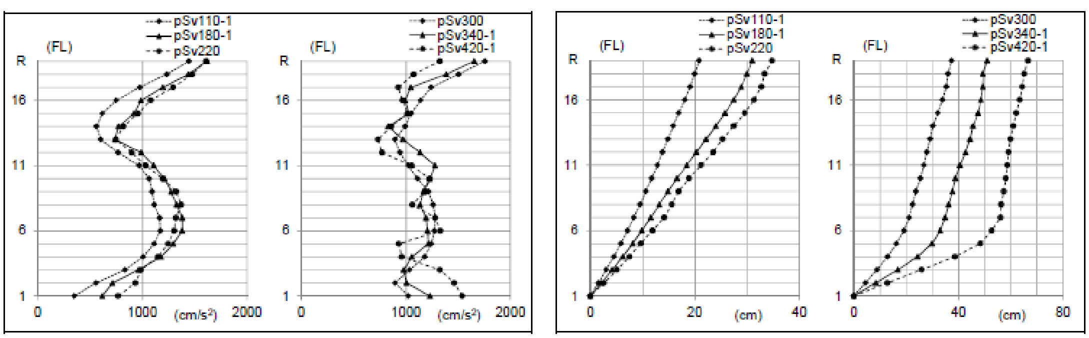

(a) Absolute acceleration

(b) Relative deformation

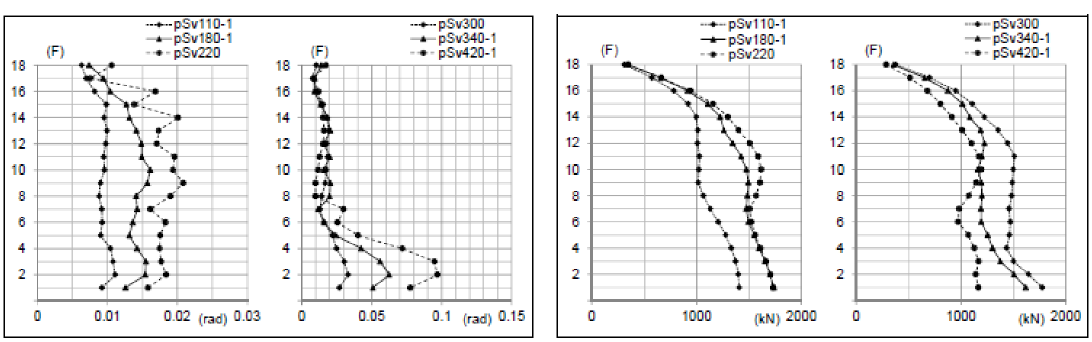

(c) Story drift angle

(d) Story shear force

Fig. 8 – Maximum response distribution

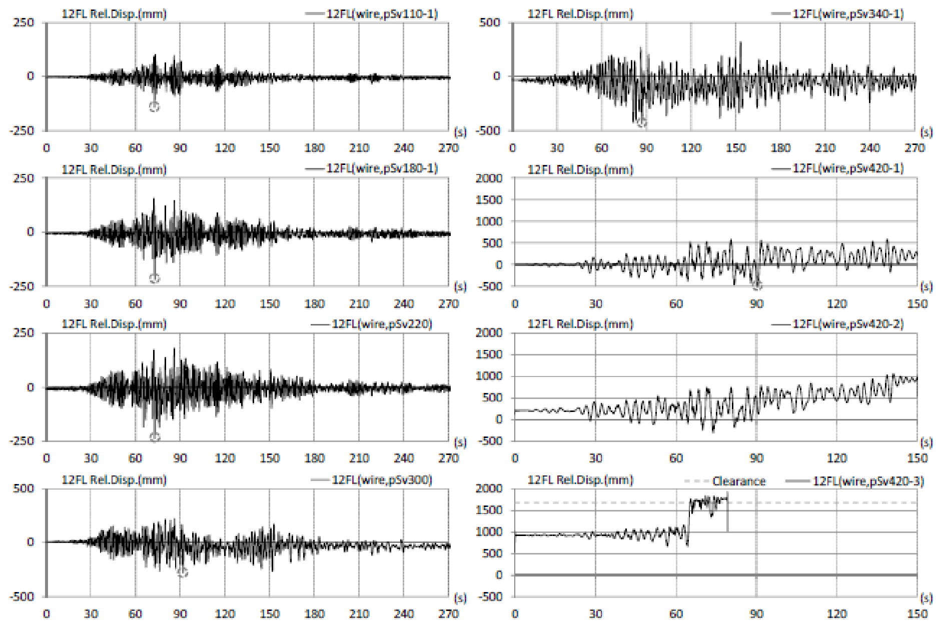

Fig. 9 – Time history of 12th floor deformation

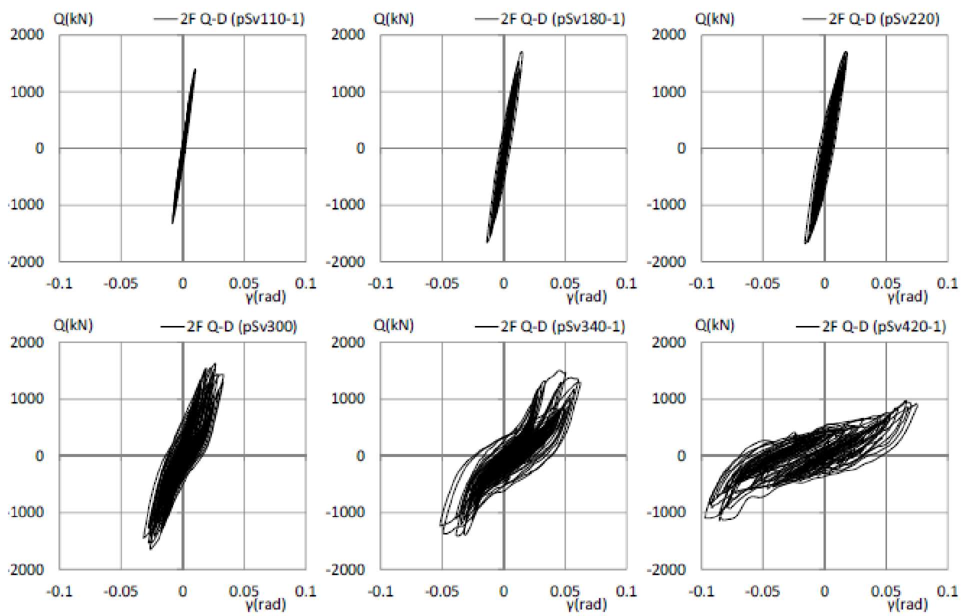

Fig. 10 – Relationships between story shear force and drift angle (second story)

4.3 Behavior of beams

The relationships between the beam moment and rotation angle observed at the outer end beam B21 the second story are shown in Fig. 11. At an excitation level of pSv110-1, the beam ends exhibit certain levels of plasticity. In case of positive moment, the lower flange of the beam subjected to compression force, conversely, subjected to tension force in case of negative moment. At pSv180-1, the bending moment reaches full plasticity (135 kNm calculated by using steel actual tensile strength), and a large hysteresis area is observed. At pSv220, deterioration on the lower-flange tension side with lower-flange fracture is observed. Local buckling of the lower flange did not occur before the fracture. At pSv300, the moment on the lower-flange tension side is low, and a moment increase is observed when the lower flange transitions to the compression side because of re-contact of lower flanges. At pSv420-1, the progression of deterioration is seen and there is little bending resistance in both of positive and negative side due to fracture of upper and lower flanges.

The fracture of the beam end after tests is shown in Fig. 12. The crack occurred from the toe of the weld access hole and propagated along the weld of the beam flange. Finally, not only the lower and upper flange but also the shear plate and web fractured at the beam end connection as shown in Fig. 12(a)

4.4 Behavior of columns

The relationships between the moment and axial force of the outer column C21 and the inner column C22 are shown in Fig. 13. The long-term axial force ratio (i.e., the ratio of the long-term axial force against the yielding axial force) is 0.12 for the column C21 and 0.16 for the column C22 according to long-term load analysis using a static analysis model. Fig. 13 also shows a yielding surface with consideration of the correlation between the axial force and bending moment. The negative axial force corresponds to the compression stress. At an excitation level of pSv110-1, the column C21 begins to yield on the compression side, and the maximum axial force ratio is 0.52. At pSv180-1, the column C21 yields both on the compression and tension sides. The maximum ratio on the compression side is 0.58. The variation of axial force in the column C22 was smaller compared with C21, an appreciable bending moment acts and yielding is observed. After pSv300, the variation of axial force became small, because deterioration of story shear force as shown in Fig. 10. After pSv420-1, residual deformation of the specimen occurred in the direction in which the column C21 and C22 subjected to tensile axial force and the column C21 and C22 subjected to compression axial force. The relationships between the column moment and rotation angle observed at the lower end of columns in the first story at pSv420-2 are shown in Fig. 14. Column C21 and C22 deteriorate by fracture (Fig. 15(a)) and C23 and C24 deteriorate by local buckling (Fig. 15(b)).

4.5 Damage to components

The damage situation for all components is shown in Fig. 16. Yielding and fracture are observed in the beams, and the columns also exhibit yielding. The beam locations for which the measured strain at the beam ends exceeded yielding strain are marked in gray. Only one of two frames is shown here, with the results for the other frame being similar. At an excitation level of pSv110-1, the beams partially yield on stories 2–7 and 14. At pSv180-1, all beams yield and part of the lower story reveals a fully plastic moment. Lower-flange fracture instants were identified from the observed moment-rotation angle relationships and video footage, and no progression of strain was seen on the lower-flange tension side of the beam ends. At pSv220, there was fracture of second-story beams connected to outer columns. At pSv250, fracture locations were observed widely on the third story, and were also seen on the 14th story. Positions at which column stress reached the yield surface are

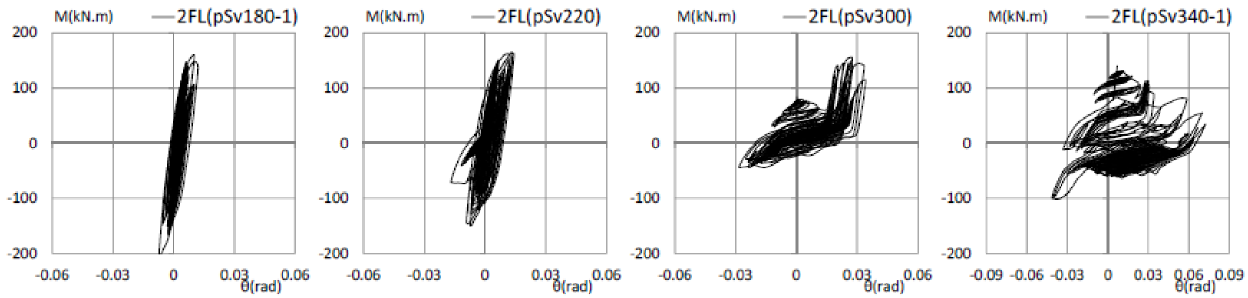

Fig. 11 – Beam M-θ Relationships (second story, B21, outer end)

(a) Beam end

(b) Lower flange

(c) Upper flange

Fig. 12 – Fracture of beam end connection

shown in gray. Plasticity was observed in the first-story outer column at an excitation level of pSv110-1 and in the outer columns on the second and fourth stories at pSv180-1. Local buckling on the first story was visually observed at pSv300.

4.6 Overall behavior during dynamic response

The bending moment distribution at the time of maximum deformation in each excitation to clarify how beam-end fracture affected the behavior of the test specimen as a whole is shown in Fig. 17. At excitation levels of

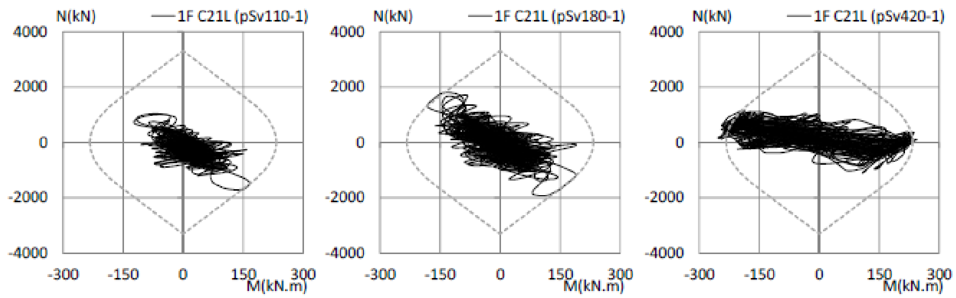

(a) first story, outer column C21, lower end

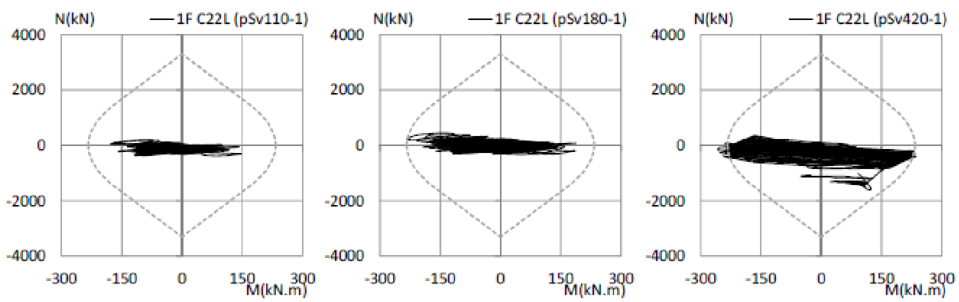

(b) first story, inner column C22, lower end

Figure 13 Column moment-axial force relationships

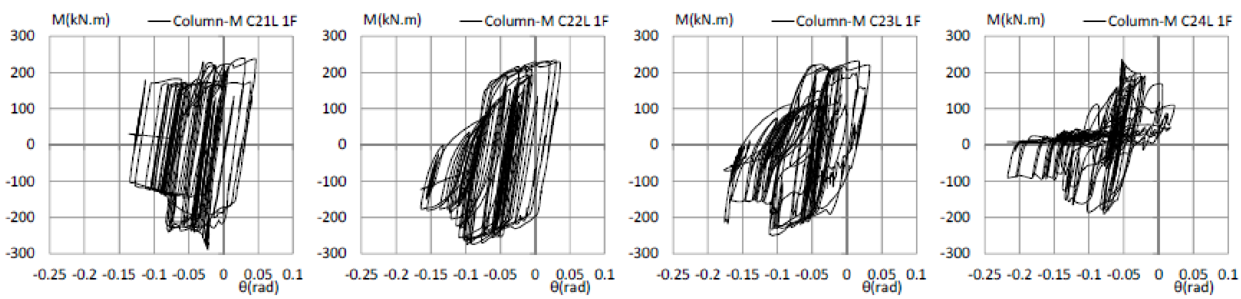

Figure 14 Column M-θ relationships (first story, lower end at pSv420-2)

(a) Fracture (b) Local buckling

Figure 15 Damage to Columns at the first story

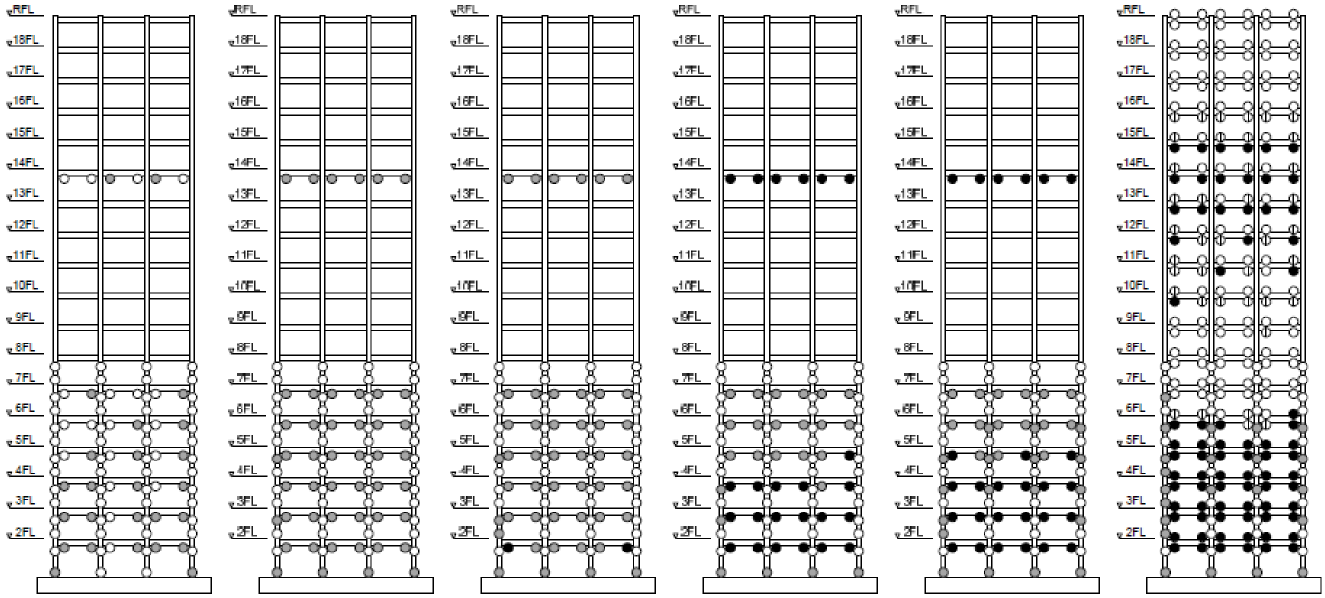

(a)pSv110-1 (b)pSv180-1 (c)pSv220 (d)pSv300 (e)pSv340-1 (f)pSv420-3

Figure 16 – Beam and column damage

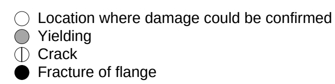

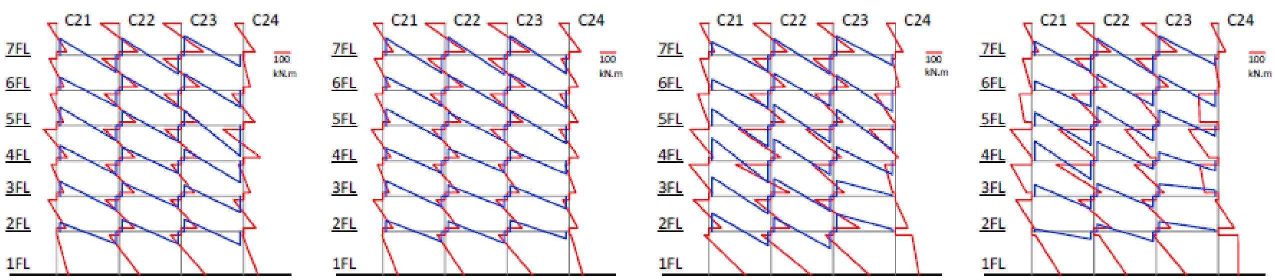

(a) pSv180-1 (b) pSv220 (c) pSv300 (d) pSv340-1

Figure 17 – Moment distribution at maximum deformation

pSv110-1 and pSv180-1, the moment distribution of beams is characterized by reverse symmetric bending, and the distribution for the columns on the second to seventh stories is characterized by almost reverse symmetric bending. The bending moment for first-story columns is extremely large because of the fixed condition of the lower ends if these columns. At pSv220, fracture occurs at beam ends connected to outer columns (C21 and C24 on the second story). The moment for beam B23, connected to column C24, is smaller. Meanwhile, the moment for beam B21, connected to column C21, is not as small because the lower flange is on the compression side and can still handle moment forces after fracture. At pSv300, a state similar to that seen at pSv220 is observed on the third story as well as on the second story. The point of contraflexure at the first to the third story of column C24 is located only at third story and the flexure length of Column C24 becomes longer. At pSv340-1, the flexure length of Column C24 extended to the fifth story. Decrease of beam moment was observed in Column C21 and inner columns C22 and C23 due to fracture of lower- and upper-flange of beam end. Shear forces of columns decreased in these stories since the extension of flexure length of Columns expanded to many columns and upper stories. Finally, the flexure length of Columns extended to the seventh story and the column shear forces decreased.

4.7 Process to collapse

From foregoing observations of test results, the process to collapse of the specimen is as follows.

According to the weak beam - strong column criteria, a plastic mechanism by yielding of multistory beams and column base at the first story is formed. Under the long-duration ground motions, due to many cycles of repeated plastic deformations at beam ends, cracks initiate at the welds of beam lower flanges and propagate along flange width followed by fracture of the lower flange. The fracture area of beam flanges extends to the upper stories and fracture of beam flanges change moment distribution of columns. The flexure length of columns elongates to multistory and shear resistance of columns deteriorates. At the upper ends and lower ends of elongated flexure length of columns, plastic hinges formed, and the deformation of the frame progressed due to the PD effect, and finally sideway collapse occurred.

5. Conclusions

At the E-Defense, a series of shaking table tests of an 18-story steel moment resisting frame was conducted until total collapse of the frame by using synthetic long-period long-duration ground motions whose source is Nankai Trough Earthquake. From the test results, hysteretic characteristics of beams and columns including deterioration due to fracture and local buckling were revealed. The process to collapse of the frame was also examined.

The damage to the steel frame began through the yielding of beams along lower stories and column bases of the first story. After several excitations by increasing scaled motions, cracks initiated at the welded moment connections and fractures in the beam flanges spread to the lower stories. As the shear strength of each story decreased, the drifts of lower stories increased and the frame finally collapsed and settled on the protective frame. The process to collapse of the specimen is as follows.

According to the weak beam - strong column criteria, a plastic mechanism by yielding of multistory beams and column base at the first story is formed. Under long-duration ground motions, due to many cycles of repeated plastic deformation at beam ends, cracks initiate at the welds of beam lower flanges and propagate along flange width followed by fracture of the lower flange. The area of fracture of beam flanges extends to the upper stories and fracture of beam flanges change moment distribution of columns. The flexure length of columns elongates to multistory and shear resistance of columns deteriorates. At the upper ends and lower ends of elongated flexure length of columns, plastic hinges formed, and the deformation of the frame progressed due to the PD effect, and finally sideway collapse occurred.

Acknowledgement

The study was conducted as part of research sponsored by Japan’s Ministry of Education, Culture, Sports, Science and Technology under the title (ii) Maintenance and Recovery of Functionality in Urban Infrastructure, which is a sub-project of the Special Project for Reducing Vulnerability in Urban Mega Earthquake Disasters. The authors are grateful to all those who are contributed to and participated in the project. Particular thanks go to Associate Prof. Yuji Koetaka of Kyoto University, to Associate Prof. Jun Iyama of The University of Tokyo and to Associate Prof. Takuya Nagae of Nagoya University, for their assistance.

5. References

[1] Nakashima M., Suita K., Takahashi M., Nishiyama M., Katsumata H., Kajiwara K., and Koshika N. Overview of ‘Quantification of collapse margin of high-rise buildings’ Quantification of collapse margin of steel high-rise buildings (Part 1), Summaries of Technical Papers from the Annual Meeting of the Architectural Institute of Japan 2013, pp. 967~968 (in Japanese).

[2] Ramos D.C., Mosqueda G., and Lignos D.G. Hybrid simulation of the seismic response of a steel moment frame building structure through collapse, Technical report MCEER-14-0003, 2014, pp. 5~18.

[3] Lignos D.G., Krawinkler H., and Whittaker A.S. Prediction and validation of sidesway collapse of two scale models of a 4-story steel moment frame, Journal of Earthquake Engineering and Structural Dynamics 2011, pp. 807~825.

[4] Suita K., Yamada S., Tada N., Kasai K., Matsuoka Y., and Sato E. E-Defense tests on full-scale steel buildings(Part 2) Collapse experiments on moment frames, Proceedings of Structural Engineering Research Frontiers, ASCE, 2007.

[5] Nakashima M. Roles of large structural testing for the advance of earthquake engineering, Proceedings of the 14th World Conference on Earthquake Engineering, Beijing, China, 2008.

[6] Yu-Lin Chung, Nagae T., Matsumiya T., and Nakashima M. Seismic resistance capacity of beam-column connections in high-rise buildings, E-Defense shaking table test, Journal of Earthquake Engineering and Structural Dynamics 2011, pp.605~622.

[7] Lignos D.G. and Krawinkler H. A database in support of modeling of component deterioration for collapse prediction of steel frame structures, Proceedings of Structural Engineering Research Frontiers, ASCE, 2007.

[8] Sivaselvan M.V. and Reinhorn A.M. Hysteretic models for deteriorating inelastic structures, Journal of Engineering Mechanics, ASCE, June 2000, pp.633~640.

[9] Ibarra L.F., Medina R.A., and Krawinkler H. Hysteretic models that incorporate strength and stiffness deterioration, Earthquake Engineering and Structural Dynamics, Volume 34, October 2005, pp.1489~1511.

[10] Tada M., Ohsaki M., Yamada S., Motoyui S., and Kasai K. E-Defense tests on full-scale steel buildings (Part3) Analytical simulation of collapse, Proceedings of Structural Engineering Research Frontiers, ASCE, 2007.

[11] Kato B. and Akiyama H. The ultimate strength of the steel beam-column(Part 4), Journal of Structural and Construction Engineering, Architectural Institute of Japan, 1968, pp.15~20 (in Japanese).

[12] Lavan O., Sivaselvan M.V., and Reinhorn A.M., Dargush G.M. Progressive collapse analysis through strength degradation and fracture in the mixed lagrangian framework, Proceedings of the 14th World Conference on Earthquake Engineering, Beijing, China, 2008.

[13] Lignos D.G., Hikino T., Matsuoka U., and Nakashima M. Collapse assessment of steel moment frames based on E-Defense full-scale shake table collapse tests, Journal of Structural Engineering, ASCE, June 2013, pp.120~132.

[14] Suita K., Nakashima M., and Engelhardt M.D. Comparison of seismic capacity between Post-Northridge and Post-Kobe beam-to-column connections, Proceedings of the Third International Conference on Behavior of Steel Structures in Seismic Areas (STESSA), Montreal, Canada, pp. 271~278.

[15] Sato T, Okawa I, Nishikawa T, Sato T, Seki M. Prediction of waveforms of long-period ground motions for hypothetical earthquakes using empirical regression relations of response spectra and phase spectra , Journal of Structural and Construction Engineering, Architectural Institute of Japan, 2010, 649, 521 - 530 (in Japanese).